NASA TECHNICAL NOTE

NASA TN D-4475

NASA TN D-4475

AMPTIAC

OXIDE DEFORMATION AND FIBER REINFORCEMENT IN A TUNGSTEN - METAL-OXIDE COMPOSITE

by Charles P. Blankenship

Lewis Research Center
Cleveland, Ohio

NATIONAL AERONAUTICS AND SPACE ADMINISTRATION • WASHINGTON, D. C. • MARCH 1968

NASA TN D-4475

OXIDE DEFORMATION AND FIBER REINFORCEMENT IN A TUNGSTEN - METAL-OXIDE COMPOSITE

By Charles P. Blankenship

Lewis Research Center
Cleveland, Ohio

NATIONAL AERONAUTICS AND SPACE ADMINISTRATION

For sale by the Clearinghouse for Federal Scientific and Technical Information
Springfield, Virginia 22151 – CFSTI price $3.00

OXIDE DEFORMATION AND FIBER REINFORCEMENT IN A TUNGSTEN - METAL-OXIDE COMPOSITE

by Charles P. Blankenship

Lewis Research Center

SUMMARY

From p. 2

Refractory oxide particles of urania (UO_2) and zirconia (ZrO_2) were added to a tungsten matrix yielding 20 v/o composites and elongated into fibers by hot extrusion. Extrusion temperatures ranged from 3200° to 4000° F (1760° to 2200° C). The geometry of the oxide fibers appeared to be closest to that of an ellipsoid with the major axis alined in the extrusion direction. Oxide fibering was measured by an average length-to-width ratio $\bar{\lambda}_L$ of the fibers sectioned parallel to the major axis. The extent of oxide deformation was estimated in terms of strain components. Oxide-matrix deformation characteristics were related to the extrusion parameters by comparing the estimated oxide strain components to those of the composite.

In terms of fibering, the greatest oxide elongation $\bar{\lambda}_L \cong 200$, was obtained in tungsten-UO_2 composites extruded at 3600° F (1980° C) with a composite reduction of 18 to 1. Values of $\bar{\lambda}_L$ for tungsten-UO_2 composites extruded at 3200° and 4000° F (1760° and 2200° C) were nearly equal ($\bar{\lambda}_L \cong 100$) even though the composite reductions were 12 to 1 and 18 to 1, respectively. For a tungsten-ZrO_2 composite extruded at 4000° F (2200° C), $\bar{\lambda}_L \cong 160$. These length-to-width ratio values have no direct relation to the length-to-diameter ratio commonly used to describe fibered composites containing cylindrical fibers.

Comparison of estimated oxide and composite strain components showed that oxide deformation in the tungsten-UO_2 composites (parallel to extrusion direction) approached that of the composite at temperatures of 3200° and 3600° F (1760° and 1980° C). At 4000° F (2200° C) the matrix had a greater tendency to flow around the stronger oxide particles resulting in UO_2 deformation less than that of the composite. Under similar processing conditions at 4000° F (2200° C), ZrO_2 exhibited greater deformation parallel to the extrusion direction than UO_2 and approached that of the composite.

Tungsten-UO_2 composites with $\bar{\lambda}_L \cong 200$ had tensile strengths about twice that of additive-free tungsten at 3500° F (1930° C), approximately 14 000 and 7000 pounds per square inch (96.5 and 48.2 MN/m^2), respectively. Composites having $\bar{\lambda}_L \cong 100$ were about 30 percent stronger than additive-free tungsten. The greater strength of the composites was attributed to fiber reinforcement. Fibers of UO_2 appeared to be stronger than those of ZrO_2.

End

INTRODUCTION

Direct fabrication of fibered composites was demonstrated in two studies conducted at this center (refs. 1 and 2). Equiaxed, refractory compounds (oxides, carbides, etc.), added to a tungsten or to a columbium matrix, were elongated into fibers by hot extrusion as illustrated in figure 1. Fabricating fibered composites by this method avoids two of the conditions limiting attempts to improve the strength of refractory metals by fiber metallurgy techniques. First, suitable fibers are not available. Secondly, deterioration of fiber properties may be encountered at the high temperatures required for incorporating fibers into a refractory metal matrix.

Composites prepared by the extrusion process contain discontinuous fibers. Reinforcement with discontinuous fibers requires at least a minimum fiber length or length-to-diameter ratio (refs. 3 and 4). Meeting this requirement in extruded composites depends upon the additive-matrix deformation characteristics. Probably, the most important factor is the relative flow stresses of the additive and matrix for a given amount of plastic strain at the temperature of deformation. Also, additive concentration and particle size will affect the extent of fibering.

The objectives of this investigation were threefold; they are as follows:

(1) To examine fibering of refractory oxide particles in extruded tungsten composites

(2) To define oxide-matrix deformation characteristics with respect to extrusion parameters

(3) To correlate composite strengths with the extent of oxide fibering

Additives of urania (UO_2) and zirconia (ZrO_2) with melting points near 5000° F (2760° C) were selected for this study. A 20 volume percent additive concentration was selected to yield a representative composite.

In the previous studies cited, the composites were extruded through conical dies in the form of bar stock. While this is the most direct approach, nonhomogeneous deformation (which is characteristic of the extrusion process) results in greater plastic strain at the periphery of the extrusion than at the center (ref. 5). In order to approach conditions of uniform deformation, attempts were made to extrude the tungsten composites in the form of thin-wall tubing. Nominal tubing dimensions were selected to be either 5/8 or 1/2 inch (16 or 13 mm) outside diameter with wall thicknesses of either 0.030 or 0.020 inch (0.76 or 0.51 mm). Attempts were made to extrude the composites at temperatures ranging from 2800° to 4600° F (1540° to 2550° C) with nominal composite reductions of either 18 to 1 or 12 to 1. The extruded composites were examined for dimensional variations, density, and uniformity of oxide deformation. Composite tensile strengths, determined at 3500° F (1930° C), are compared to additive-free tungsten which was extruded and tested under similar conditions.

SYMBOLS

a, b, c	length of reference axes of ellipsoid
a_o, b_o, c_o	length of reference axes of sphere
C	coefficient of variation
D	fiber diameter
fv	volume fraction of oxide particles
K_l, K_r, K_θ	deformation indices
L	length of fiber overlap needed to transmit shear stresses equal to tensile stress on fiber
l	final length
l/w	fiber length-to-width ratio
l_o	initial length
MFP	mean free path
n_L	total number of particles measured parallel to extrusion direction
n_T	total number particles measured perpendicular to extrusion direction
P_L	number of oxide particles intersected per unit length of random lines
S	standard deviation
V_E	volume of ellipsoid
V_S	volume of sphere
γ	load transfer constant, $\sigma_f/4\tau$
ϵ	natural strain
$\epsilon_l, \epsilon_r, \epsilon_\theta$	composite strain components
$\epsilon_X, \epsilon_Y, \epsilon_Z$	oxide strain components
λ_L	fiber l/w parallel to extrusion direction
$\bar{\lambda}_L$	average fiber l/w parallel to extrusion direction (used as measure of oxide fibering)
λ_T	fiber l/w perpendicular to extrusion direction
$\bar{\lambda}_T$	average fiber l/w perpendicular to extrusion direction
σ_f	fiber tensile strength

σ_u ultimate tensile strength

τ shear strength of fiber-matrix interface

MATERIALS AND PROCEDURE

Extrusion Billet Design and Preparation

Billet design for extrusion of composite tubing is shown schematically in figure 2. Canning the composites reduces the effective reduction required for direct extrusion of thin-wall tubing. In addition, the canning materials should absorb the large surface strains associated with friction at the billet-tooling interfaces resulting in more uniform deformation of the composites. The molybdenum or molybdenum alloy components of the 2-inch (51-mm) nominal-diameter billets were fabricated by powder-metallurgy techniques and sintered to a density of 90 to 95 percent of theoretical.

Composite cylinder dimensions which are dependent upon the final tubing size were calculated assuming fully dense billet components. Two methods were used in preparing the tungsten-composite cylinders. For extrusion of 5/8-inch-diameter (16-mm-diam.) tubing, $3\frac{1}{2}$-inch-long (89-mm-long) cylinders were prepared by conventional powder-metallurgy techniques of dry blending the powders, hydrostatic pressing, and sintering. Urania, available in the form of spherical powder, was used in most studies for ease in characterizing deformation. The average particle size of the spherical UO_2 and the irregularly shaped ZrO_2 was 45 microns. The average particle size of the tungsten was 0.88 micron. After composite consolidation by hydrostatic pressing at 50 000 pounds per square inch (345 MN/m^2), the cylinders were sintered in a hydrogen atmosphere at 3200° F (1760° C) for 4 hours. The 85 to 90 percent dense cylinders (as measured by mercury displacement) were ground to the required outside diameter of 1.740 inches (44.2 mm) and inside diameter of 1.320 inches (33.6 mm). Four cylinders of this size containing 20 volume percent UO_2 and two containing 20 volume percent ZrO_2, were canned in molybdenum for extrusion over 0.50-inch-diameter (13-mm-diam.) mandrels at a nominal reduction of 18 to 1.

Smaller composite cylinders were required for the extrusion of 1/2-inch-diameter (13-mm-diam.) tubing at a nominal reduction of 12 to 1. These cylinders, with 1.150 inch (29.2 mm) outside diameter by 0.900 inch (22.8 mm) inside diameter, were prepared by closed-die compaction. The metal and oxide powders (tungsten, 4.5 μm; spherical UO_2, 45 μm) were dry blended and vibratorily compacted into a steel, piston-type compaction billet shown in figure 3. Prior to hot compaction, the pistons were forced into the billets under a pressure of 130 000 pounds per square inch (895 MN/m^2). This increased the precompaction density to approximately 70 percent of theoretical.

Six billets prepared in this manner were compacted in a high velocity forging and extrusion press at temperatures near 2200° F (1200° C). Compaction pressures were estimated to be near 250 000 pounds per square inch (1725 MN/m^2). After compaction, the billets were furnace cooled and the steel cans were removed by chemical dissolution. All of the composite cylinders exhibited transverse and longitudinal cracks. Cracking was presumed to have resulted from the stresses induced by the larger thermal contraction of the steel cans. However, four of the 3-inch-long (76-mm-long) cylinders were considered to be suitable for extrusion since the extent of oxide deformation was of primary interest. After a postheat treatment in hydrogen for cleaning (1 hr at 3000° F or 1650° C), the composites were canned in either molybdenum - 25-percent-tungsten or molybdenum - 3-percent-columbium for extrusion over 0.40-inch-diameter (10.2-mm-diam.) mandrels.

Composites prepared by the closed-die compaction process exhibited a high degree of particle bonding, densification, and uniformity. Composite densities were from 95 to 97 percent of theoretical, and a typical composite structure is shown in figure 4.

Extrusion of Composite Tubing

The metal-oxide composites were extruded in a vertical extrusion press equipped with 2-inch (51-mm) nominal-diameter tooling. Press operation, tooling design, and accessories for extrusion at the relatively high temperatures used herein are described in reference 6. Processing details for extrusion of tubing are described in reference 7. Extrusion temperatures for the composites ranged from 2800° to 4600° F (1500° to 2550° C).

Composite Evaluation

After removal of the canning material, the extruded composite tubing was examined for dimensional variations. Samples for density measurements were taken from the middle and from random locations along the tube lengths.

Tensile specimens conforming to figure 5 were cut from tube samples by electrical discharge machining. The majority of the test specimens were cut from random locations along the tube lengths. Tensile tests were conducted in vacuum at a pressure of 5×10^{-5} torr (7.7×10^{-3} N/m^2). The specimens were heated to a test temperature of 3500° F (1930° C) in 1 hour, and the tests were conducted at a crosshead speed of 0.03 inch (0.76 mm) per minute. The testing apparatus is similar to that described in reference 8.

Analysis of Oxide and Composite Deformation

Deformation of the oxide particles contained in the composite tubing translated the particles into a geometry closely approaching that of an ellipsoid. The major axis of the ellipsoid is parallel to the extrusion direction. Oxide fibering is measured by an average length-to-width ratio l/w of the fibers sectioned parallel to the major axis. This ratio has no direct relation to the length-to-diameter ratio commonly used to describe fibered composites containing cylindrical fibers. Oxide deformation is estimated in terms of strain components using average l/w measurements as outlined in the following sections. The deformation characteristics of the oxide and the matrix are related to the extrusion parameters by comparing the estimated oxide strain components to those of the composite.

Determination of strain components. - For the extruded composite tubing, oxide-matrix deformation characteristics were evaluated by comparing oxide strain components to those of the composite. The strain analysis is similar to that presented in reference 9 for rolled steel containing nonmetallic inclusions. By using natural strain defined by the instantaneous change in length, that is,

$$\epsilon = \int_{l_o}^{l} \frac{dl}{l} = \ln \frac{l}{l_o} \tag{1}$$

and by following the coordinate system illustrated in figure 6, the strain components of the oxide particles can be defined as follows.

If the oxide particles are assumed to be perfect spheres and are translated into ellipsoids during extrusion, the l/w parallel and perpendicular to the extrusion direction (λ_L and λ_T, respectively) are

$$\left.\begin{aligned} \lambda_L &= \frac{a}{c} \\ \text{and} \\ \lambda_T &= \frac{b}{c} \end{aligned}\right\} \tag{2}$$

Assuming the oxide volume does not change during deformation, then the volume of the sphere

$$V_S = \frac{4\pi}{3} a_o b_o c_o \tag{3}$$

and the volume of the ellipsoid

$$V_E = \frac{4\pi}{3} abc \tag{4}$$

are equal, that is,

$$V_S = V_E \tag{5}$$

From equation (1), the strain in the extrusion direction is defined as

$$\epsilon_X = \ln \frac{a}{a_o} \tag{6}$$

By substituting the values of a and a_o from equations (3) and (4) into equation (6) and by introducing from equation (2)

$$a = \lambda_L c \quad \text{and} \quad b = \lambda_T c$$

the following solution for ϵ_X is obtained:

$$\epsilon_X = \frac{1}{3} \ln\left(\frac{\lambda_L^2}{\lambda_T}\right) \tag{7}$$

Similarly, it can be shown that the other strain components ϵ_Y and ϵ_Z can be defined as

$$\epsilon_Y = \frac{1}{3} \ln\left(\frac{\lambda_T^2}{\lambda_L}\right) \tag{8}$$

and

$$\epsilon_Z = \frac{1}{3} \ln\left(\frac{1}{\lambda_T \lambda_L}\right) \tag{9}$$

Thus, the principal strain components are defined in terms of particle deformation parallel and perpendicular to the extrusion direction.

Correspondingly, the plastic strain components of the composite, with reference to figure 6, are given by the following relations:

$$\epsilon_l = \ln \frac{l}{l_o} \quad \text{(axial strain)} \tag{10}$$

$$\epsilon_r = \ln \frac{t}{t_o} \quad \text{(radial strain)} \tag{11}$$

and

$$\epsilon_\theta = \ln \frac{r}{r_o} \quad \text{(tangential strain)} \tag{12}$$

where ϵ_l, ϵ_r, and ϵ_θ correspond to the particle strain components in the X, Y, and Z directions, respectively. Although the particle and composite strain components are derived from different coordinate systems, any error introduced is assumed to be negligible since the particles are minute in reference to the composite. This appears to be reasonable since the strains are assumed to be independent of the strain path and since only initial and final dimensions are used to determine the composite strain components. For the particles, strain is defined only by the final l/w measurements.

Deformation indices were used to compare the oxide deformation to that of the composite. These indices were based on the ratio of corresponding strain components and are defined as follows:

$$\left.\begin{aligned} K_l &= \frac{\epsilon_X}{\epsilon_l} \\ K_r &= \frac{\epsilon_Z}{\epsilon_r} \end{aligned}\right\} \tag{13}$$

and

$$K_\theta = \frac{\epsilon_Y}{\epsilon_\theta}$$

The values of these indices can range from zero up to unity for oxide deformation either less than or equal to that of the composite. Index values greater than unity indicate oxide deformation greater than that of the composite. The index K_l can be used as a measure of the efficiency of oxide fibering.

Data measurements. - Values of λ_L and λ_T were measured from metallographic samples taken from the center and from random locations along the tube lengths. For measuring λ_L, samples sectioned parallel to the extrusion direction were photographed at a magnification of 50 and enlarged four times. Length measurements on the photographs were made within 0.02 inch (0.5 mm) and width measurements were made with a magnified scale which permitted measurement within 0.002 inch (0.05 mm). Where required, several areas of the same sample were photographed so that at least 50 particles were measured in determing representative values of λ_L for the sample. For measuring λ_T, samples sectioned perpendicular to the extrusion direction were photographed at a magnification of 100 and enlarged four times. Three random lines were inscribed on the photographs, and λ_T was measured for each particle intersected by the lines using the magnified scale.

If the oxide particles are assumed to be ellipsoids after deformation, then the l/w measurement is the true l/w of the particle provided the sample is sectioned parallel or perpendicular to the elliptical axes. Deviations in sample sectioning and particles deviating from an elliptical shape will result in an experimental error. There will be some variation in λ_L and λ_T because of differences in particle size and other factors which might result in nonuniform deformation. In addition, oxide deformation will vary from the nose to the tail of the extrusion because of temperature variations during the extrusion process. Therefore, for determining λ_L and λ_T of a particular composite, all of the l/w measurements were averaged. The $\bar{\lambda}_L$ of a composite was used as a measure of oxide fibering.

Normally, to determine an average oxide strain component, λ_L and λ_T of each particle would be substituted into the proper strain equation and all of the strain values averaged. However, λ_L and λ_T were measured independently and not for the same particle. Substituting the values of $\bar{\lambda}_L$ and $\bar{\lambda}_T$ into the proper strain equation may yield the average strain component if $\bar{\lambda}_L$ and $\bar{\lambda}_T$ are representive of the sample population.

In this study, an approach based on the distribution of the measured values of λ_L and λ_T was used to estimate the oxide strain components. The method of analysis is presented in the appendix along with a statistical treatment of the procedure to determine the accuracy of the estimated strain components.

The effective composite strain components were calculated from the initial and final dimensions of the extruded composites. The composite strain components were considered to be average values.

The mean-free-path (MFP) between oxide particles (perpendicular to the extrusion direction) was determined by lineal analysis using the relation

$$MFP = \frac{1 - fv}{P_L}$$

(ref. 10) where the term fv stands for the volume fraction of the particles and P_L represents the number of particles intersected per unit length of random lines inscribed on the enlarged photographs.

RESULTS AND DISCUSSION

Extrusion of Tungsten-Composite Tubing

Data obtained from extrusion of the composite tubing are summarized in table I. Billets WC-1 and WC-2, containing the tungsten-ZrO_2 composites, were extruded at 4300° and 4000° F (2370° and 2200° C), respectively. Billet WC-1 required 66 percent of the press capacity (200 000 psi (1380 MN/cm^2) for 2-in.-diam. (51-mm-diam.) tooling) and extruded at an average speed of 144 inches per second (336 cm/sec). Although the tubing remained intact, considerable surface tearing was encountered during extrusion which extended to, and in some areas, through the composite tube wall. Apparently, the combination of extrusion temperature and speed was excessively high for the molybdenum-canned composite. Billet WC-2, extruded at 4000° F (2200° C), required a higher pressure, but the extrusion speed decreased to 72 inches per second (184 cm/sec). In addition to an improved surface finish, the tubing was sound and uniform. A section of the composite tubing after removal of the molybdenum is shown in figure 7(a).

The pressed and sintered tungsten-UO_2 composites were extruded at either 4000° F (2200° C) (billets WC-3 and WC-4) or 3600° F (1980° C) (billets WC-5 and WC-6). All four extrusions were integrally sound, close to size, and fairly uniform. However, the composites extruded at 3600° F (1980° C) exhibited better surface finishes indicating that the molybdenum can-composite flow characteristics were more compatible at the lower extrusion temperature. Similar results were observed in the extrusion of tungsten tubing canned in molybdenum (ref. 7). A representative section of tubing from this group is shown in figure 7(b).

Attempts were made to extrude billets WC-7 to WC-10, containing the tungsten-UO_2 composites fabricated by closed-die compaction, at temperatures either higher or lower than those previously used. Billet WC-8 was extruded successfully at 3200° F (1760° C). Even though the composite cylinder was cracked, the extruded tubing was integrally

sound and fairly uniform as shown in figure 7(c). Billet WC-7, heated to a temperature of 2800° F (1540° C), could not be extruded at maximum press capacity. Billets WC-9 and WC-10, extruded at temperatures of 4400° and 4600° F (2430° and 2540° C), respectively, did not yield integrally sound tubing. Even though the composites were canned in a molybdenum - 25-percent-tungsten alloy (mp, ~5000° F or ~2760° C), the temperatures encountered during extrusion resulted in tearing of the canning material, melting at the can-composite interface, and nonuniform deformation of the tubing. From this group, only composite WC-8 provided samples which were suitable for analysis of oxide deformation.

Dimensional data of the composite tubing, after removal of the canning material, are summarized in table I. The tubing dimensions were close to the calculated values. Dimensional deviations were not greater than ±0.005 inch (±0.13 mm). Those composites successfully extruded were fully dense as determined by mercury displacement and by metallographic examination.

Oxide and Composite Deformation

Metallographic observations. - In examining oxide and composite deformation, attention was given to the preextrusion composite density and to the flow pattern of the oxide particles during extrusion. For this purpose, billet WC-3 was extruded partially, and the butt was sectioned for metallographic examination. These results, presented in figure 8, indicate that the composite completely densified during billet upset prior to entering the die orifice. Along with the increase in density, the dimensions of the composites were altered slightly. Part of the dimensional change was associated with composite densification and part with the increase in billet diameter during upset into the extrusion liner. Measurements of the composite in the extrusion butt indicated a 3 percent diametrical increase and a 1/2 percent decrease in wall thickness. These changes are noted since they introduce a slight error in the calculation of composite strain components and the composite reduction. The cracks present in the extrusion butt shown in figure 8 were introduced while stripping the composite from the extrusion liner.

Photomicrographs of the oxide flow pattern show some particle-to-particle contact as the extrusion passes through the die orifice (fig. 8). Particle-to-particle contact resulted from the inability to disperse the oxide particles uniformly in the metal matrix by blending of powders. However, most of the oxide particles are separated entities throughout the extrusion process, and only those particles were included in the ℓ/w measurements.

Representative microstructures of the extruded composites are shown in figures 9 to 12. In all of the composites, the oxide additives plastically deformed with no evidence

of fracture. Even in the composite containing irregularly shaped ZrO_2 particles, the geometry of the deformed oxided perpendicular to the extrusion direction (figs. 9(a), 10(a), 11(a), and 12(a)) was close to being elliptical as assumed in the derivation of strain components. The greatest deviation from an elliptical shape was shown by composite WC-8 (fig. 12(a)). The uniformity of oxide deformation parallel to the extrusion direction is illustrated in figures 9(b), 10(b), 11(b), and 12(b) which show at least 90 percent of the composite wall thicknesses. These figures also show the extent of oxide fibering parallel to the extrusion direction. As indicated in these figures, oxide fibering as measured by $\bar{\lambda}_L$ ranged from about 100 to 200 depending on the extrusion temperature and the composite reduction. Oxide deformation was more uniform in the composites having $\bar{\lambda}_L \cong 200$ (fig. 11(b)) indicating a closer match of oxide-matrix deformation characteristics. Compared to the transverse sections, the fiber geometry parallel to the extrusion direction does not appear to conform as closely to an elliptical shape. However, with the relatively large l/w ratios, the fibers would have a slow rate of decreasing thickness from center to the ends. This would give the appearance of a nearly constant width along the central portions of the fibers with decreasing thickness towards the ends. Some of the fibers exhibited an irregular thickness.

In all of the composites, the tungsten matrices were recrystallized with no evidence of matrix porosity or oxide-matrix reactions. There was some variation in matrix grain size depending on the extrusion temperature. Tungsten-UO_2 composites extruded at 3600° F (1980° C) exhibited a matrix grain size about one-half that of similar composites extruded at 4000° F (2200° C) (figs. 10(c) and 11(c), respectively). From comparison of figures 11(c) and 12(c), an extrusion temperature of 3200° F (1760° C) resulted in a matrix grain size approximately one-half that of the composites extruded at 3600° F (1980° C). No definite reason was established for the larger grain size of the tungsten-ZrO_2 composite compared to that of the tungsten-UO_2 composites extruded under similar conditions (figs. 9(c) and 10(c), respectively).

Deformation characteristics. - Oxide and composite deformation in terms of l/w measurements, strain components, and deformation indices are summarized in table II. From the aspect of fibering, the greatest oxide elongation ($\bar{\lambda}_L \cong 200$) was obtained in the tungsten-UO_2 composites extruded at 3600° F (1980° C) (WC-5 and WC-6). Values of $\bar{\lambda}_L$ for the tungsten-UO_2 composites extruded at 4000° F (2200° C) (WC-3 and WC-4) and for the tungsten-UO_2 composite extruded at 3200° F (1760° C) (WC-8) were nearly equal (approximately 100), even though the composite reductions were 18 to 1 and 12 to 1, respectively. The pronounced effect of temperature on oxide fibering is related to the relative resistances to deformation of the oxide and the matrix. Values of $\bar{\lambda}_T$, ranging from about 5 to 7, were not as greatly affected by extrusion parameters.

The oxide strain components, listed in table II, are estimated values as determined by the procedure outlined in the appendix. The statistical analysis of the strain data are

presented in table III in terms of the standard deviation S and the coefficient of variation C of the respective strain components. The relatively small values of S and C compared to the mean strain components shows that the method of analysis gives a fairly accurate estimate of the oxide strain. In addition to processing variables, possible errors in the analysis include the deviations of the particles from a spherical geometry, and deviations of the deformed oxides from an ellipsoidal geometry. However, the author has considered the analysis in terms of strain components assuming a fiber geometry of an ellipsoid to be the most representative of the deformation process.

In terms of axial strain and axial deformation indices, oxide deformation in the tungsten-UO_2 composites (WC-3, WC-4, WC-5, and WC-6) increased and approached that of the composite as the extrusion temperature was lowered from 4000° to 3600° F (2200° to 1980° C). Radial and tangential components also show greater oxide deformation at the lower extrusion temperature. Radial deformation indices show oxide deformation is slightly greater than that of the composite ($K_r > 1$) in all samples. Tangential deformation indices show oxide deformation to be less than that of the composite. Deformation indices for the composites WC-2 and WC-8 exhibited strain relations similar to the other composites with axial deformation of the oxide and the composite nearly equal.

To obtain long fiber lengths, the strain component in the principal working direction is most important. In this respect, the deformation index K_l is useful as a measure of the efficiency of fibering. If it is assumed that oxide deformation cannot exceed that of the composite, K_l values of unity would indicate maximum efficiency. Fibering in composites WC-2, WC-5, WC-6, and WC-8 was closest to maximum efficiency. K_l could have values greater than unity depending upon the stress state during deformation. However, to maintain displacement continuity, the matrix would be subjected to the same amount of strain. Accordingly, the other strain components would change to maintain continuity. Values of K_r greater than unity suggest oxide deformation greater than that of the composites in the radial direction. Others have reported inclusion deformation greater than that of the bulk sample in the principle direction of working (refs. 9, 11, and 12).

Characterization of oxide deformation on the basis of strain components illustrates the complex flow that occurs in the deformation of composite materials. In addition, the strain components are indicative of the complex stress states associated with the extrusion process. These results suggest that deformation of the components in a composite material is dependent upon the relative flow stresses of the components for a given amount of strain at the temperature of deformation. For the tungsten-UO_2 composites, the oxide has a greater flow stress than the matrix at 4000° F (2200° C) resulting in a greater tendency for the matrix to flow around the oxide particles. At 3600° F (1980° C), the relative increase in the flow stress of the matrix was greater than that of the oxide and defor-

mation of the latter was increased. Comparison of oxide deformation in the composites extruded at 4000° and 3200° F (2200° and 1760° C) also demonstrates the change in component flow stresses with temperature. Even though the composite reduction was less at 3200° F (1760° C) (i.e., 12 to 1), oxide deformation was nearly as great as that obtained in the composites extruded at 4000° F (2200° C) with reduction of 18 to 1. Temperature variations within a composite during extrusion were found to affect the extent of oxide deformation in a similar manner. For example, values of $\bar{\lambda}_L$ for the nose, center, and tail sections of composite WC-5 were 178, 214, and 220, respectively. These data are in accord with the decrease in billet temperature due to contact with the tooling. The tail section, being the last part of the billet to be extruded, is in contact with the tooling for a longer period of time and deformation occurs at a lower temperature.

Comparison of the strain components for the tungsten-UO_2 and tungsten-ZrO_2 composites extruded under similar conditions (WC-2, WC-3, and WC-4) shows that UO_2 has a greater resistance to deformation than ZrO_2 at 4000° F (2200° C). The relative ease in which ZrO_2 was deformed in a tungsten matrix compared to other attempts to fiber ZrO_2 in a similar manner (ref. 1) is probably related to particle size. Oxide deformation was less in extruded tungsten-ZrO_2 composites containing 5 to 20 volume percent 2-micron-diameter ZrO_2. Since neither the composite reduction nor the volume fraction of oxide were indentical to that of composite WC-2, a direct comparison of results cannot be made. However, with the larger oxide particle size (45 μm), greater forces can be generated at the oxide-matrix interface since the larger particles offer greater resistance to matrix flow. This would account for the greater deformation of the larger ZrO_2 particles used in this study.

Composite Tensile Properties

The tensile strengths of the composites and additive-free tungsten at 3500° F (1925° C) are presented in table IV. The tensile strength of the additive-free tungsten, approximately 7000 pounds per square inch (48.2 MN/m^2), is in close agreement with the reported strength of wrought sintered tungsten tested under similar conditions (ref. 8). Tungsten-UO_2 composites with the greatest oxide fibering ($\bar{\lambda}_L \cong 200$) were about twice as strong as additive-free tungsten. Composites with oxide fibering near 100 were only about 30 percent stronger than additive-free tungsten. Test results from composite WC-5 also show the dependence of composite tensile strength on oxide fibering. Specimens having greater $\bar{\lambda}_L$ values exhibited higher tensile strengths (except for the one specimen not considered to be representative).

The greater strengths of the composites is attributed to fiber reinforcement. The dependence of composite strength on fiber l/w is related to fiber length and to fiber

strength. In the composites containing fibers with greater l/w values, the longer fiber lengths provide more effective load transfer from the matrix to the fibers by shear. In addition, the fibers with greater l/w values could be stronger because of the greater deformation (reduction in size) to which they were subjected.

The average of the measured fiber lengths for $\bar{\lambda}_L \cong 200$ was about 600 microns. For $\bar{\lambda}_L \cong 100$, the average of the measured fiber lengths was about 400 microns. Because of the fiber geometry, the fibers were not always sectioned through the major axis where the fiber length is maximum. Therefore, average fiber lengths are greater than the measured values. For an ideal ellipsoid, the average length obtained from an infinite number of sections parallel to the major axis (with lengths of zero to the maximum) was calculated to be about 0.8 of the length of the major axis. On this basis, average fiber lengths for $\bar{\lambda}_L = 200$ would be about 750 microns. Average lengths for $\bar{\lambda}_L \cong 100$ would be about 500 microns. Attempts to remove the fibers from the composites to confirm particle length and geometry were unsuccessful.

Metallographic analysis of the tensile fractures shows evidence of strengthening by fiber reinforcement. Composites having l/w values near 100 exhibited extensive matrix deterioration by grain boundary void formation adjacent to the fractures (fig. 13(a)). Composites having l/w values near 200 showed negligible matrix deterioration (fig. 14(a)). These results illustrate that the tensile load was transferred more effectively from the matrix to the fibers in those composites having greater l/w values. The fracturing of the fibers at and adjacent to the specimen failure is evidence that the fibers were subjected to a tensile load and that excellent bonding was achieved between the fibers and the matrix. In all of the composites the matrix fractures were intergranular (figs. 13(b) and 14(c)).

Although the tungsten-ZrO_2 composite exhibited greater values of $\bar{\lambda}_L$ than the tungsten-UO_2 composites extruded under similar conditions, there was no appreciable difference in strength. From the limited number of tests made, these data suggest that the UO_2 fibers were stronger than those of ZrO_2. The greater resistance to deformation of UO_2 than ZrO_2 (at 4000° F or 2200° C) is consistent with this observation.

Since the oxide particle size in the extruded composites is too large for dispersion strengthening (particle sizes of 0.1 μm are required (ref. 13)) and since no matrix-oxide reactions were observed, matrix grain size appears to be the only other factor which could contribute to the observed strengthening. Grain size was shown to affect the strength of unalloyed tungsten with fine grain structures exhibiting higher tensile strengths (ref. 14). The grain size of the composites extruded at 3600° F (1980° C) was approximately one-half that of those extruded at 4000° F (2200° C). After the 3500° F (1930° C) tensile tests, the grain size of the composites extruded at 3600° F (1980° C) were about one-tenth of those extruded at 4000° F (2200° C) (figs. 13(b) and 14(b)), respectively). On a comparative basis, the smaller grain size of the stronger composites

would provide a moderate increase in strength since decreasing grain size by a factor of 20 increased the tensile strength of arc cast and extruded tungsten by 40 percent at 3500° F (1930° C) (ref. 14).

The greater resistance to grain growth in the composites extruded at 3600° F (1980° C) is probably related to the interfiber spacing. The MFP in the composites extruded at 3600° F (1980° C) was 15 and 17 microns. In the composites extruded at 4000° F (2200° C), the MFP was 19 and 23 microns. Since the volume fraction of oxide was the same in all of the composites, the smaller MFP in the stronger composites with larger ℓ/w values resulted from more particle overlap.

FIBER-MATRIX LOAD TRANSFER CONSTANT

In composites containing discontinuous fibers, the load is transferred from fiber to fiber by shear through the matrix. To use the greater strength of the fibers, shear failure of the matrix or matrix-fiber interface must be prevented. Therefore, the ratio of the tensile strength of the fibers to the shear strength of the interface can be used as a measure of the ability of the fiber to fail in tension rather than having shear failure at the interface. By equating the shear load of the fiber-matrix interface to the tensile load necessary to cause failure of the fiber, this ratio for cylindrical fibers was shown to be represented by (ref. 3)

$$\frac{\sigma_f}{4\tau} = \frac{L}{D}$$

where

σ_f tensile strength of fiber

τ shear strength of fiber-matrix interface or shear strength of matrix whichever is less

L length of fiber overlap needed to transmit shear stress equal to tensile stress on fiber

D fiber diameter

A similar analysis was made for the fiber geometry in the extruded composites. For this purpose, the fibers were assumed to be rods with an elliptical cross section. In terms of $\bar{\lambda}_L$ and $\bar{\lambda}_T$, the ratio of tensile strength to shear strength or load transfer constant γ is given by

$$\gamma = \frac{\sigma_f}{4\tau} = \frac{\bar{\lambda}_L}{\bar{\lambda}_T}\sqrt{\frac{\bar{\lambda}_T^2 + 1}{2}}$$

For composites with $\bar{\lambda}_L \cong 200$, γ would be about 150. For composites with $\bar{\lambda}_L \cong 100$, γ would be about 75.

CONCLUDING REMARKS

Additional studies are required to determine the strength of fibers contained in the extruded tungsten composites. Only an estimate can be made with the limited data available. To estimate fiber strengths, it is assumed that the rule of mixtures (ref. 3) applies to the tungsten-UO_2 composites; that is, the composite strength is a linear function of the fiber content and of the ultimate tensile strength of the fibers. Secondly, it is assumed that fiber lengths greater than 600 microns exceed the critical length such that the average tensile stress on each fiber approaches that of continuous length fibers. Then, the tensile strength of the UO_2 fibers could be as high as 42 000 pounds per square inch (290 MN/m^2) at 3500° F (1930° C).

Although fiber reinforcement of tungsten was demonstrated, the tensile strength of the composites at 3500° F (1925° C) is not comparable to the better tungsten alloys (refs. 15 and 16). Additional studies are required to assess the potential use of oxide fibers for reinforcing tungsten.

SUMMARY OF RESULTS

Oxide fibering and oxide-matrix deformation characteristics were studied in extruded tungsten composites. Refractory oxide particles of zirconia (ZrO_2) and urania (UO_2) were added to a tungsten matrix and elongated into fibers by hot extrusion. The fiber geometry appeared to be closest to that of an ellipsoid with the major axis alined parallel to the extrusion direction. Oxide fibering was measured by an average length-to-width ratio $\bar{\lambda}_L$ of the fibers sectioned parallel to the extrusion direction. This ratio has no direct relation to the length-to-diameter ratio commonly used to describe fibered composites containing cylindrical fibers. This study was conducted in relation to the fabrication of fiber reinforced composites; the results are summarized as follows:

1. Maximum fibering was obtained in tungsten-UO_2 composites extruded at 3600° F (1980° C) with a composite reduction of 18 to 1. For these composites, $\bar{\lambda}_L \cong 200$. Values of $\bar{\lambda}_L$ for tungsten-UO_2 composites extruded at 3200° and 4000° F (1750° and

2200° C) were nearly equal (approximately 100) even though the composite reductions were 12 to 1 and 18 to 1, respectively. For a tungsten ZrO_2 composite extruded at 4000° F (2200° C), $\bar{\lambda}_L \cong 160$.

2. Comparison of estimated oxide and composite strain components showed that oxide deformation in the tungsten-UO_2 composites (parallel to the extrusion direction) approached that of the composite at extrusion temperatures of 3200° and 3600° F (1760° and 1980° C). At 4000° F (2200° C) the matrix had a greater tendency to flow around the stronger oxide particles resulting in UO_2 deformation less than that of the composite. Under similar processing conditions at 4000° F (2200° C), ZrO_2 exhibited greater deformation than UO_2 and approached that of the composite.

3. Tungsten-UO_2 composites having $\lambda_L \cong 200$ exhibited tensile strengths about twice that of additive-free tungsten at 3500° F (1930° C), approximately 14 000 pounds per square inch (96.5 MN/m^2) and 7000 pounds per square inch (48.2 MN/m^2), respectively. Composites having $\bar{\lambda}_L \cong 100$ were about 30 percent stronger than additive free tungsten. The greater strength of the composites was attributed to fiber reinforcement. The UO_2 fibers appeared to be stronger than those of ZrO_2.

Lewis Research Center,
National Aeronautics and Space Administration,
Cleveland, Ohio, November 13, 1967,
129-03-14-03-22.

APPENDIX - PROCEDURE FOR ESTIMATING OXIDE STRAIN COMPONENTS

The procedure outlined in this appendix was used to estimate the average of the oxide strain components for each composite and to determine the accuracy of the method of analysis.

For the i^{th} particle measured parallel to the extrusion direction

$$\lambda_{Li} = \frac{L_{Li}}{W_{Li}} \tag{A-1}$$

and for the j^{th} particle measured perpendicular to the extrusion direction

$$\lambda_{Tj} = \frac{L_{Tj}}{W_{Tj}} \tag{A-2}$$

With reference to equation (7) the axial strain is defined as

$$\epsilon_{Xij} = \frac{1}{3} \ln \left[\frac{(\lambda_{Li})^2}{\lambda_{Tj}} \right] \tag{A-3}$$

or

$$\epsilon_{Xij} = \frac{2}{3} \ln \lambda_{Li} - \frac{1}{3} \ln \lambda_{Tj} \tag{A-4}$$

From a preliminary examination of the data, $\ln \lambda_{Li}$ and $\ln \lambda_{Tj}$ were found to have a more normal distribution, whereas values of λ_{Li} and λ_{Tj} exhibited an asymmetrical distribution (fig. 15). This type of relation was observed in the deformation of inclusions during rolling of steel and was considered to be justification for using natural strain as the characteristic measure of inclusion deformation (ref. 9). Therefore, since $\ln \lambda_{Li}$ and $\ln \lambda_{Tj}$ appear to be more representative of the oxide deformation and since λ_L and λ_T are independent measurements, the average strain components were estimated by an arithmetical average of the individual measurements in logarithmic form. With reference to equation (A-4), then

$$\bar{\epsilon}_X = \frac{2}{3}\frac{1}{n_L}\sum_{i=1}^{n_L} \ln \lambda_{Li} - \frac{1}{3}\frac{1}{n_T}\sum_{j=1}^{n_T} \ln \lambda_{Tj} \tag{A-5}$$

where n_L and n_T are the number of particles measured parallel and perpendicular to the extrusion direction, respectively.

Similarly, the average of the other strain components can be estimated by the following relations:

$$\bar{\epsilon}_Y = -\frac{1}{3}\frac{1}{n_L}\sum_{i=1}^{n_L} \ln \lambda_{Li} + \frac{2}{3}\frac{1}{n_T}\sum_{j=1}^{n_T} \ln \lambda_{Tj} \tag{A-6}$$

and

$$\bar{\epsilon}_Z = -\frac{1}{3}\frac{1}{n_L}\sum_{i=1}^{n_L} \ln \lambda_{Li} - \frac{1}{3}\frac{1}{n_T}\sum_{j=1}^{n_T} \ln \lambda_{Tj} \tag{A-7}$$

To determine the accuracy of estimating average strain components by the previous relations, the data were treated statistically. Both the standard deviation S and the coefficient of variation C were used as the measure of accuracy. By definition (ref. 17) the standard deviation S of λ_L can be expressed as

$$S_L^2 = \frac{\sum_{i=1}^{n_L} \ln \lambda_{Li}^{\,2} - \frac{1}{n_L}\left(\sum_{i=1}^{n_L} \ln \lambda_{Li}\right)^2}{n_L - 1} \tag{A-8}$$

and the standard deviation of λ_T can be expressed as

$$S_T^2 = \frac{\sum_{j=1}^{n_T} \ln \lambda_{Tj}^{\,2} - \frac{1}{n_T}\left(\sum_{j=1}^{n_T} \ln \lambda_{Tj}\right)^2}{n_T - 1} \tag{A-9}$$

where the right-hand side of equations (A-8) and (A-9) is the variance. Since the variance of a sum of uncorrelated variables is equal to the sum of the variance (ref. 17), the standard deviation of the strain components can be expressed as follows:

$$S^2_{\epsilon_X} = \left(\frac{2}{3}\right)^2 \frac{S_L^2}{n_L} + \left(\frac{1}{3}\right)^2 \frac{S_T^2}{n_T} \tag{A-10}$$

$$S^2_{\epsilon_Y} = \left(\frac{1}{3}\right)^2 \frac{S_L^2}{n_L} + \left(\frac{2}{3}\right)^2 \frac{S_T^2}{n_T} \tag{A-11}$$

and

$$S^2_{\epsilon_Z} = \left(\frac{1}{3}\right)^2 \frac{S_L^2}{n_L} + \left(\frac{1}{3}\right)^2 \frac{S_T^2}{n_T} \tag{A-12}$$

The coefficient of variation defined as

$$C = \frac{S}{\epsilon} \tag{A-13}$$

expresses the standard deviation as a fraction of the sample mean. Values of C were determined for all of the strain components and are expressed as a percentage.

REFERENCES

1. Quatinetz, Max; Weeton, John W.; and Herbell, Thomas P.: Studies of Tungsten Composites Containing Fibered or Reacted Additives. NASA TN D-2757, 1965.
2. Jech, Robert W.; Weeton, John W.; and Signorelli, Robert A.: Fibering of Oxides in Refractory-Metal Matrices. NASA TN D-3923, 1967.
3. McDanels, David L.; Jech, Robert W.; and Weeton, John W.: Stress-Strain Behavior of Tungsten-Fiber-Reinforced Copper Composites. NASA TN D-1881, 1963.
4. Kelley, A.; and Tyson, W. R.: Fiber-Strengthened Materials. High-Strength Materials. V. F. Zackay, ed., John Wiley and Sons, Inc., 1965, pp. 578-602.
5. Pearson, Claude E.; and Parkins, Redvers N.: The Extrusion of Metals. Second ed., John Wiley and Sons, Inc., 1960.
6. Gyorgak, Charles A.: Extrusion at Temperatures Approaching 5000° F. NASA TN D-3014, 1965.
7. Blankenship, Charles P.; and Gyorgak, Charles A.: Extrusion of 1/2- and 3/8-Inch-Diameter, Thin-Wall Tungsten Tubing Using the Floating-Mandrel Technique. NASA TN D-3772, 1966.
8. Sikora, Paul F.; and Hall, Robert W.: Effect of Strain Rate on Mechanical Properties of Wrought Sintered Tungsten at Temperatures Above 2500° F. NASA TN D-1094, 1961.
9. Malkiewicz, T.; and Rudnik, S.: Deformation of Non-Metallic Inclusions During Rolling of Steel. J. Iron Steel Inst., vol. 201, pt. 1, Jan. 1963, pp. 33-38.
10. Underwood, E. E.: Quantitative Metallography. ASM Metals Eng. Quart., vol. 1, no. 3, Aug. 1961, pp. 70-81; and no. 4, Nov. 1961, pp. 62-71.
11. Warrick, R. J.; and Van Ulack, L. H.: Plastic Deformation of Non-Metallic Inclusions Within Ductile Metals. Trans. ASM, vol. 57, no. 3, Sept. 1964, pp. 672-689.
12. Pickering, F. B.: Some Effects of Mechanical Working on the Deformation of Non-Metallic Inclusions. J. Iron Steel Inst., vol. 189, pt. 2, June 1958, pp. 148-159.
13. Cremens, Walter S.: Use of Submicron Metal and Nonmetal Powders for Dispersion-Strengthened Alloys. Ultrafine Particles. W. E. Kuhn, ed., John Wiley and Sons, Inc., 1963, pp. 457-478.

14. Klopp, William D.; Witzke, Walter R.; and Raffo, Peter L.: Effects of Grain Size on Tensile and Creep Properties of Arc-Melted and Electron-Beam-Melted Tungsten at 2250° F to 4140° F. Trans. AIME, vol. 233, no. 10, Oct. 1965, pp. 1860-1866.

15. Raffo, Peter L.; Klopp, William D.; and Witzke, Walter R.: Mechanical Properties of Arc-Melted and Electron-Beam-Melted Tungsten-Base Alloys. NASA TN D-2561, 1965.

16. Raffo, Peter L.; and Klopp, William D.: Mechanical Properties of Solid-Solution and Carbide-Strengthened Arc-Melted Tungsten Alloys. NASA TN D-3248, 1966.

17. Hoel, Paul G.: Introduction to Mathematical Statistics. Second ed., John Wiley and Sons, Inc., 1954.

TABLE I. - SUMMARY OF TUNGSTEN-COMPOSITE TUBING EXTRUSION DATA

Composite identity	Composition	Canning material	Nominal tube diameter		Nominal reduction ratio	Extrusion temperature		Percent of press capacity required[a]	Extrusion speed[b]		Extruded length		Outside diameter[d]				Wall thickness[d]				Length	
													Average		Deviation		Average		Deviation			
			in.	mm		°F	°C		in./sec	cm/sec	in.	cm	in.	mm	in.	mm	in.	mm	in.	mm	in.	cm
WC-1	W-20 vol. % ZrO_2	Mo	5/8	16	18 to 1	4300	2370	66	144	366	40	101	-----	-----	-----	-----	-----	----	-----	----	--	---
WC-2	W-20 vol. % ZrO_2	↓	↓	↓	↓	4000	2200	72	72	184	46	117	0.620	15.75	±0.005	±0.13	0.032	0.81	±0.003	0.08	42	107
WC-3	W-20 vol. % UO_2					4000	2200	63	108	274	32	81	.630	16.00	↓	↓	.030	.76	.003	.08	32	81
WC-4	↓					4000	2200	61	22	56	52	132	.630	16.00			.027	.69	.003	.08	42	107
WC-5						3600	1980	85	(c)	(c)	52	132	.630	16.00			.026	.66	.002	.05	42	107
WC-6						3600	1980	72	54	137	50	127	.632	16.05			.028	.71	.003	.08	42	107
WC-7		Mo-3Cb	1/2	13	12 to 1	2800	1540	100	0	0	--	---	-----	-----	-----	-----	-----	----	-----	----	--	---
WC-8		Mo-3Cb	↓	↓	↓	3200	1760	(c)	(c)	(c)	32	81	.495	12.60	±.005	±.13	.018	.46	.002	.05	26	66
WC-9		Mo-25W				4400	2430	85	66	168	34	86	-----	-----	-----	-----	-----	----	-----	----	--	---
WC-10	↓	Mo-25W				4600	2540	96	32	81	28	71	-----	-----	-----	-----	-----	----	-----	----	--	---

[a]Maximum press capacity with 2-in. (50-mm) nominal-diameter tooling, 200 000 psi (1380 MN/m^2).
[b]Average ram speed × reduction ratio.
[c]Not recorded.
[d]After removal of canning material.

TABLE II. - SUMMARY OF OXIDE-COMPOSITE DEFORMATION CHARACTERISTICS

Composite identity	Composition	Extrusion temperature		Actual reduction ratio	Average fiber l/w parallel to extrusion direction, $\bar{\lambda}_L$	Average fiber l/w perpendicular to extrusion direction, $\bar{\lambda}_T$	Axial strain		Tangential strain		Radial strain		Deformation indices[a]		
		°F	°C				$\bar{\epsilon}_X$	ϵ_l	$\bar{\epsilon}_Y$	ϵ_θ	$\bar{\epsilon}_Z$	ϵ_r	K_l	K_θ	K_r
WC-2	W-20 vol. % ZrO_2	4000	2200	18 to 1	159	5.7	2.75	2.88	-0.54	-1.29	-2.22	-1.97	0.95	0.42	1.13
WC-3	W-20 vol. % UO_2	4000	2200	18 to 1	101	5.3	2.51	2.88	-.52	-1.02	-1.99	-1.95	.87	.51	1.02
WC-4	↓	4000	2200	17 to 1	127	5.7	2.60	2.82	-.51	-.98	-2.09	-1.89	.92	.52	1.11
WC-5		3600	1980	21 to 1	208	7.1	2.91	3.05	-.57	-1.02	-2.34	-2.08	.95	.56	1.13
WC-6	↓	3600	1980	18 to 1	203	5.5	2.96	2.90	-.70	-1.00	-2.26	-1.97	1.02	.70	1.15
WC-8		3200	1760	12 to 1	98	5.7	2.42	2.44	-.37	-.83	-2.05	-1.61	.99	.45	1.27

[a]$K_l = \bar{\epsilon}_X/\epsilon_l$, $K_\theta = \bar{\epsilon}_Y/\epsilon_\theta$, and $K_r = \bar{\epsilon}_Z/\epsilon_r$.

TABLE III. - SUMMARY OF STATISTICAL ANALYSES OF OXIDE STRAIN COMPONENTS

Composite identity	Strain component	Average strain	Standard deviation, S	Coefficient of variation, C, percent	Total number of particles measured perpendicular to extrusion direction, n_T	Total number of particles measured parallel to extrusion direction, n_L
WC-2	$\bar{\epsilon}_X$	2.75	0.02	0.9	216	202
	$\bar{\epsilon}_Y$	-.54	.02	3.7		
	$\bar{\epsilon}_Z$	-2.22	.01	.6		
WC-3	$\bar{\epsilon}_X$	2.51	0.02	0.7	635	428
	$\bar{\epsilon}_Y$	-.52	.02	3.5		
	$\bar{\epsilon}_Z$	-1.99	.01	.6		
WC-4	$\bar{\epsilon}_X$	2.60	0.02	0.9	350	397
	$\bar{\epsilon}_Y$	-.51	.02	4.7		
	$\bar{\epsilon}_Z$	-2.09	.01	.7		
WC-5	$\bar{\epsilon}_X$	2.91	0.03	0.9	431	127
	$\bar{\epsilon}_Y$	-.57	.02	4.2		
	$\bar{\epsilon}_Z$	-2.34	.02	.7		
WC-6	$\bar{\epsilon}_X$	2.96	0.03	1.1	128	114
	$\bar{\epsilon}_Y$	-.70	.04	5.2		
	$\bar{\epsilon}_Z$	-2.26	.02	1.0		
WC-8	$\bar{\epsilon}_X$	2.42	0.03	1.4	123	115
	$\bar{\epsilon}_Y$	-.37	.03	7.8		
	$\bar{\epsilon}_Z$	-2.05	.02	1.0		

TABLE IV. - TENSILE STRENGTH OF EXTRUDED TUNGSTEN AND TUNGSTEN-COMPOSITE TUBING AT 3500° F (1930° C)

Composite identity	Composition	Extrusion temperature		Average fiber l/w parallel to extrusion direction, $\bar{\lambda}_L$ [a]	Ultimate tensile strength, σ_u		Percent elongation
		°F	°C		psi	MN/m^2	
WC-2	W-20 vol. % ZrO_2	4000	2200	176	8 900	61.4	--
				143	8 500	58.5	18
WC-3	W-20 vol. % UO_2	4000	2200	123	10 500	72.4	23
				100	9 100	62.7	21
				95	9 000	62.0	21
WC-4	W-20 vol. % UO_2	4000	2200	100	9 600	66.3	16
				88	9 500	65.5	14
WC-5	W-20 vol. % UO_2	3600	1980	220	14 000	96.5	11
				220	13 400	92.4	11
				[b]<200	11 600	80.0	7
				214	14 700	101.5	11
				178	12 600	86.8	11
				178	10 750	74.2	9
WC-8	W-20 vol. % UO_2	3200	1760	85	9 000	62.0	9
				116	8 200	56.5	13
				-----	9 400	64.7	--
W2-6[c]	W	4000	2200	-----	6 100	42.0	21
					7 000	48.2	18
					7 400	51.0	18

[a] $\bar{\lambda}_L$ of sample gage length.
[b] Atypical.
[c] See ref. 7 for extrusion data.

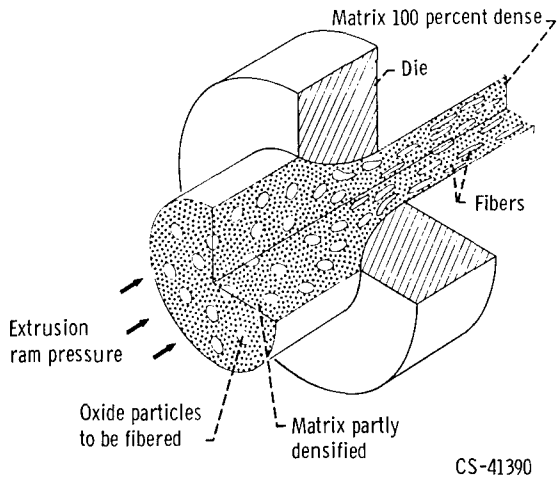

Figure 1. - Fibering of equiaxed refractory oxides by extrusion.

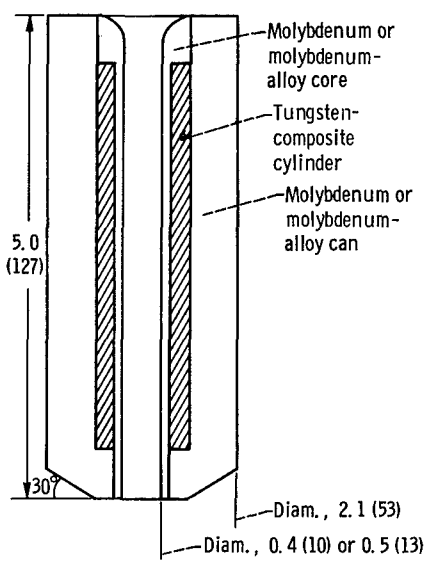

Figure 2. - Billet assembly for extrusion of tungsten-composite tubing. (Dimensions are in inches (mm) unless indicated otherwise.)

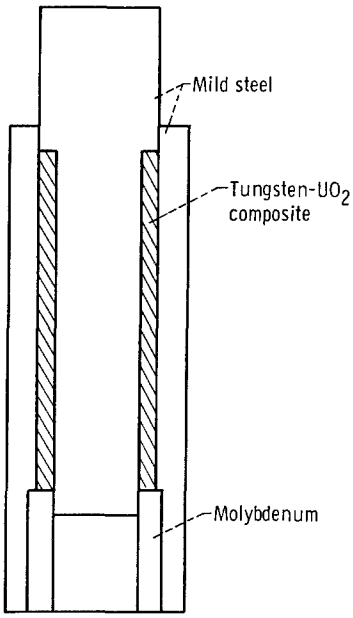

Figure 3. - Piston-type compaction billet. Diameter, 1.75 inch (44.5 mm); 0.001-inch (0.02-mm) interference fit between molybdenum and steel components.

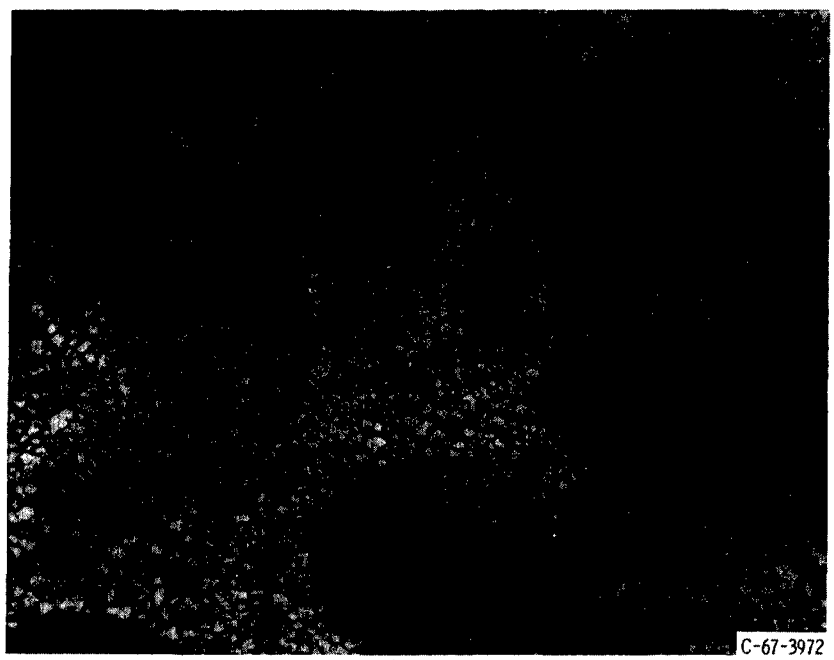

Figure 4. - Microstructure of tungsten-UO_2 composite after closed-die compaction at 2200° F (1200° C). Etchant, Murakami's reagent; x500.

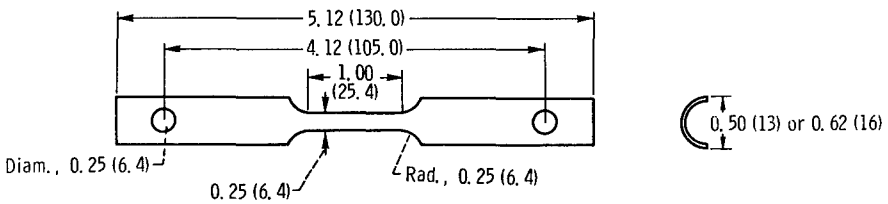

Figure 5. - Tensile specimen. (Dimensions are in inches (mm) unless indicated otherwise.)

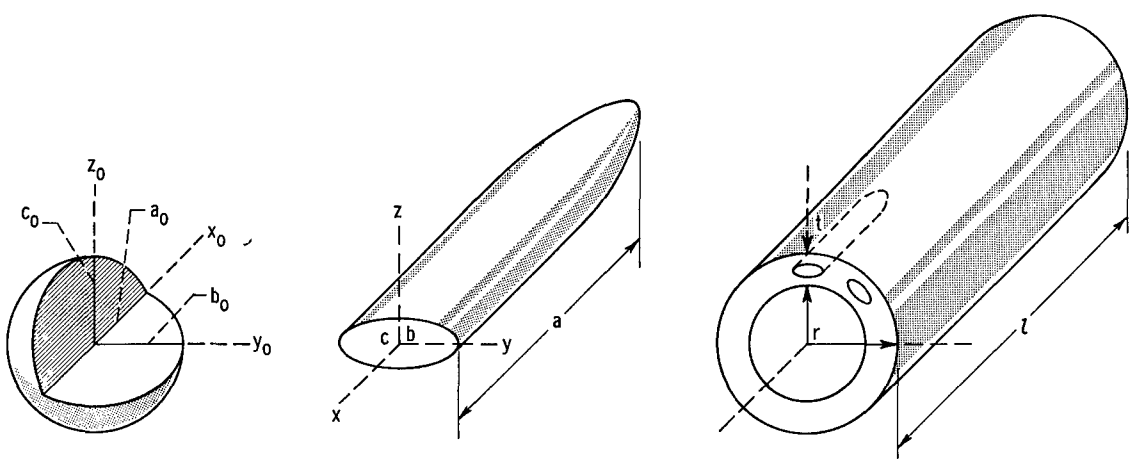

(a) Oxide particle before extrusion. (b) Oxide particle after extrusion. (c) Elongated oxide particle in extruded tube.

Figure 6. - Schematic of reference axes for comparison of oxide and composite strain components.

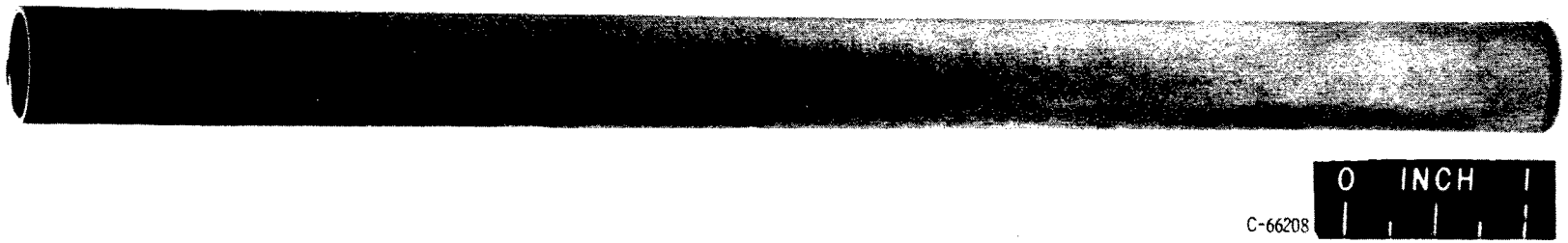

(a) Tungsten-ZrO_2 extruded at 4000° F (2200° C).

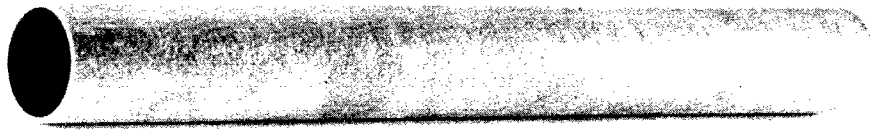

C-66461

(b) Tungsten-UO_2 extruded at 4000° F (2200° C).

C-65-576

(c) Tungsten-UO_2 extruded at 3200° F (1760° C).

Figure 7. - Representative samples of extruded composite tubing.

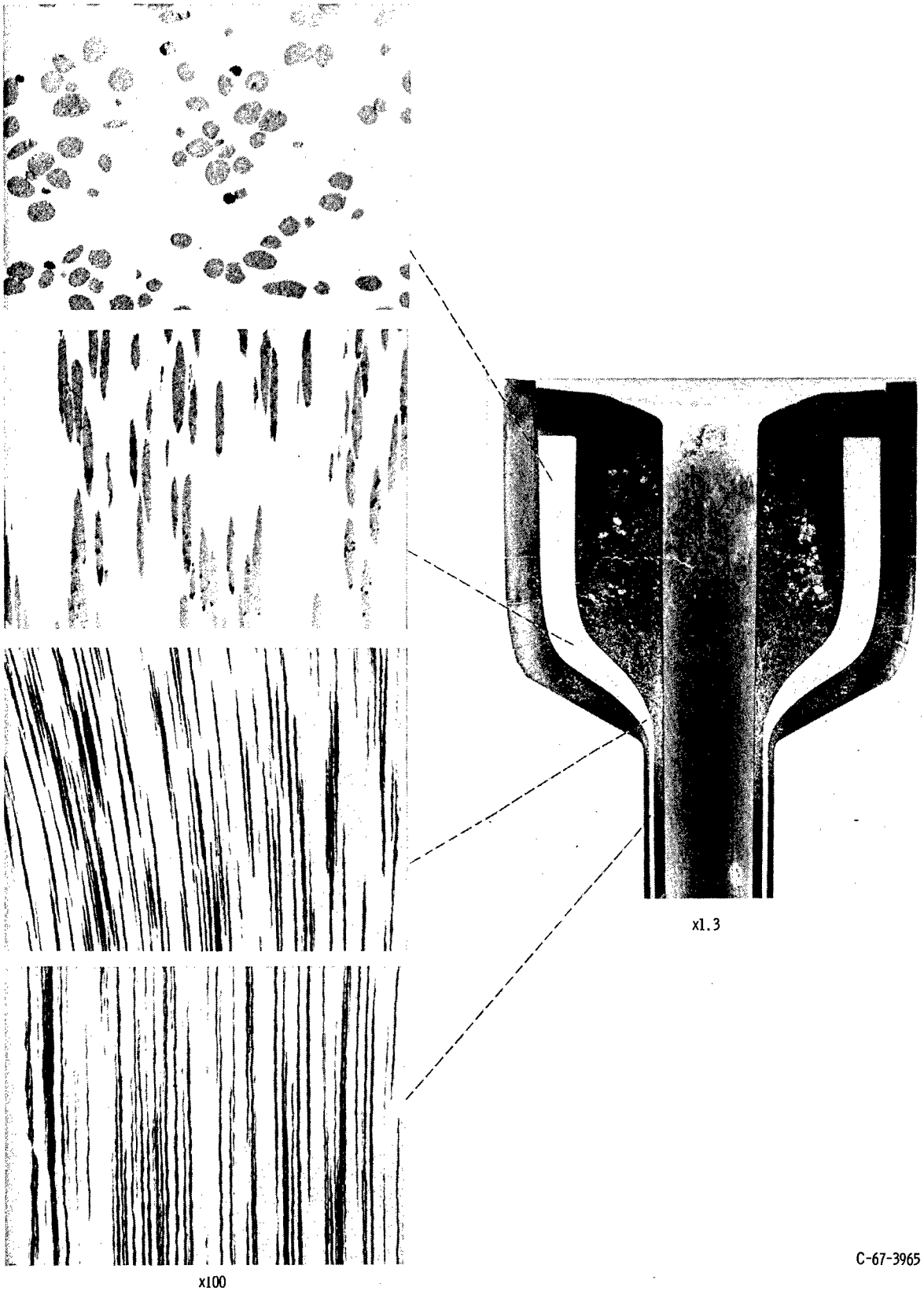

Figure 8. - Oxide deformation pattern during extrusion of composite tubing. Composite WC-3 extruded at 4000° F (2200° C).

(a) Transverse section. Unetched; x250.

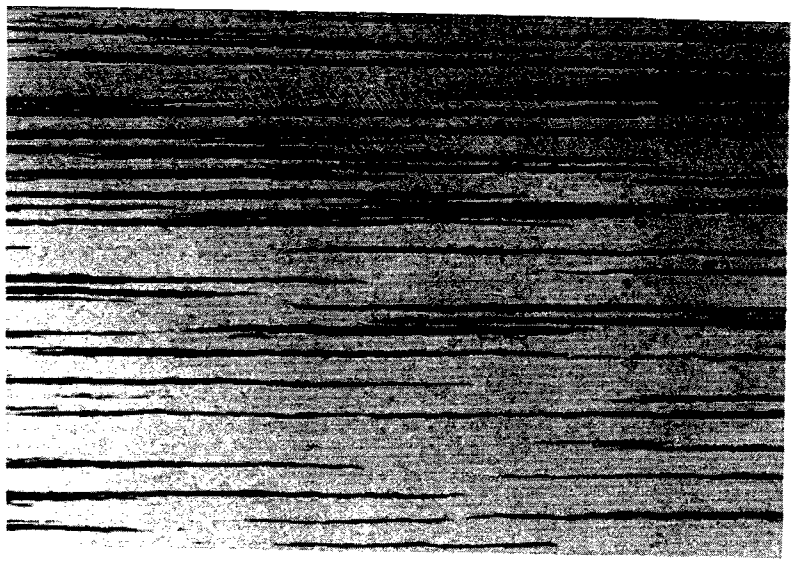

(b) Longitudinal section. Unetched; x150.

(c) Longitudinal section. Etched; x250.

Figure 9. - Microstructure of tungsten-ZrO_2 composite extruded at 4000° F (2200° C). Reduction ratio, 18 to 1; average fiber *l*/w parallel to extrusion direction, $\bar{\lambda}_L = 159$; average fiber *l*/w perpendicular to extrusion direction, $\bar{\lambda}_T = 5.7$. Etchant, Murakami's reagent.

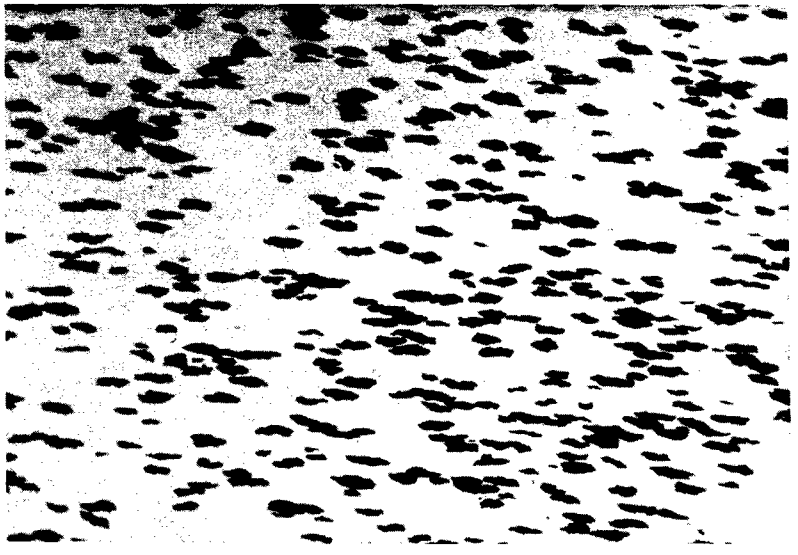

(a) Transverse section. Unetched; x250.

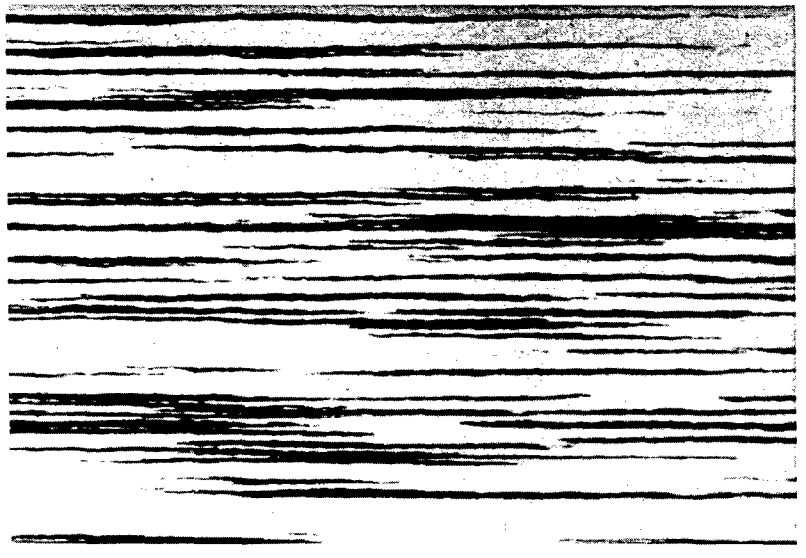

(b) Longitudinal section. Unetched; x150.

(c) Longitudinal section. Etched; x250.

Figure 10. - Microstructure of tungsten-UO_2 composite extruded at 4000° F (2200° C). Reduction ratio, 18 to 1; average fiber l/w parallel to extrusion direction, $\bar{\lambda}_L = 101$; average fiber l/w perpendicular to extrusion direction, $\bar{\lambda}_T = 5.3$. Etchant, Murakami's reagent.

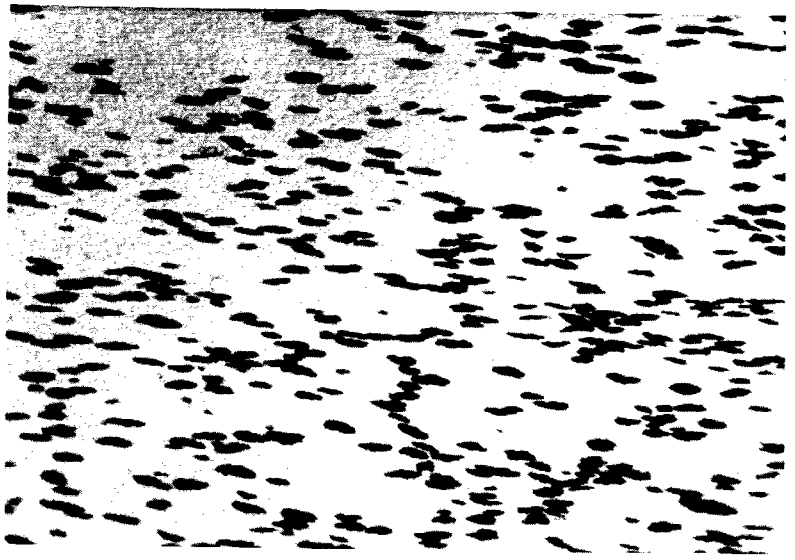

(a) Transverse section. Unetched; x250.

(b) Longitudinal section. Unetched; x150.

(c) Longitudinal section. Etched; x500.

Figure 11. - Microstructure of tungsten-UO_2 composite extruded at 3600° F (1980° C). Reduction ratio, 21 to 1; average fiber *U*w parallel to extrusion direction, $\bar{\lambda}_L$ = 208; average fiber *U*w perpendicular to extrusion direction, $\bar{\lambda}_T$ = 7.1. Etchant, Murakami's reagent.

(a) Transverse section. Unetched; x250.

(b) Longitudinal section. Unetched; x150.

(c) Longitudinal section. Etched; x250.

Figure 12. - Microstructure of tungsten-UO_2 composite extruded at 3200° F (1760° C). Reduction ratio, 12 to 1; average fiber l/w parallel to extrusion direction, $\bar{\lambda}_L = 98$; average fiber l/w perpendicular to extrusion direction, $\bar{\lambda}_T = 5.7$. Etchant, Murakami's reagent.

(a) Longitudinal section. Unetched.

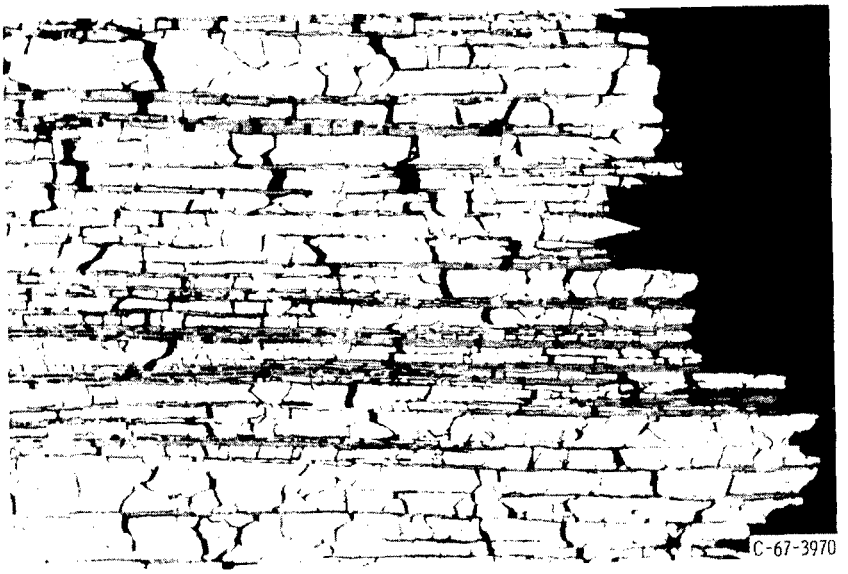

(b) Longitudinal section. Etched.

Figure 13. - Tensile fracture of tungsten-UO_2 composite at 3500° F (1930° C). Specimen WC-4 extruded at 4000° F (2200° C). Average fiber l/w parallel to extrusion direction, $\bar{\lambda}_L = 100$; ultimate tensile strength, 9600 pounds per square inch (66.3 MN/m^2). Etchant, Murakami's reagent; x150.

(a) Longitudinal section. Unetched; x150.

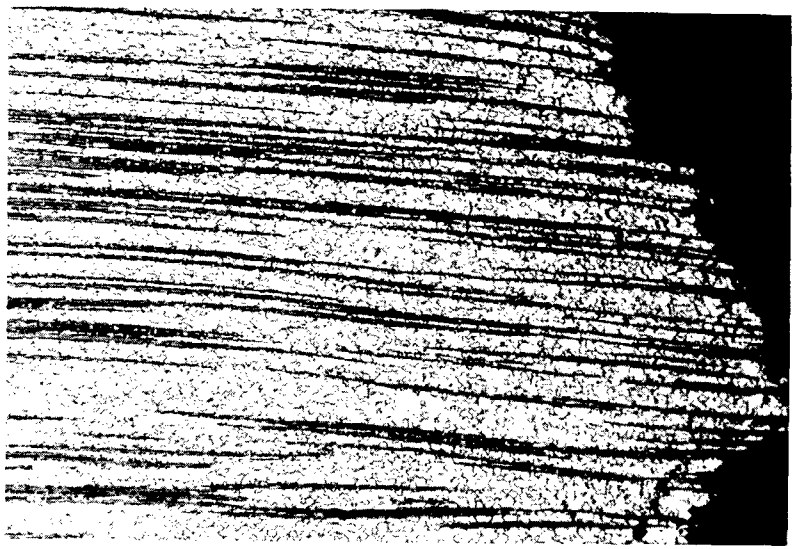

(b) Longitudinal section. Etchant, Murakami's reagent.

(c) Longitudinal section at fracture. Etchant, Murakami's reagent; x500.

Figure 14. - Tensile fracture of tungsten-U)$_2$ composite at 3500° F (1930° C). Specimen WC-5 extruded at 3600° F (1980° C). Average fiber l/w parallel to extrusion direction, $\bar{\lambda}_L$ = 220; ultimate tensile strength, 14 700 pounds per square inch (101.5 MN/m^2).

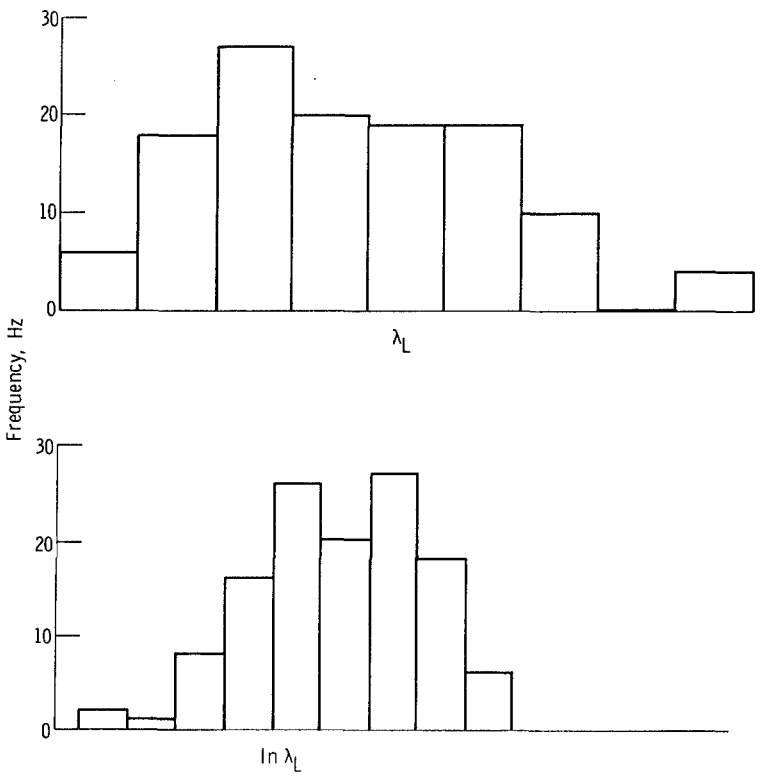

Figure 15. - Typical histograms of λ_L and ln λ_L values. (Composite WC-5 extruded at 3600° F (1980° C).)

NASA-Langley, 1968 —— 17 E-3888